



**HAL**  
open science

## Focusing choke ring antenna for a short-range millimeter-wave exposure system

Artem V. Boriskin, Maxim Zhadobov, Christian Person, Ronan Sauleau

► **To cite this version:**

Artem V. Boriskin, Maxim Zhadobov, Christian Person, Ronan Sauleau. Focusing choke ring antenna for a short-range millimeter-wave exposure system. European Microwave Conference 2013 (EuMC), Oct 2013, Nuremberg, Germany. pp.365-368. hal-00925759

**HAL Id: hal-00925759**

**<https://univ-rennes.hal.science/hal-00925759>**

Submitted on 8 Jan 2014

**HAL** is a multi-disciplinary open access archive for the deposit and dissemination of scientific research documents, whether they are published or not. The documents may come from teaching and research institutions in France or abroad, or from public or private research centers.

L'archive ouverte pluridisciplinaire **HAL**, est destinée au dépôt et à la diffusion de documents scientifiques de niveau recherche, publiés ou non, émanant des établissements d'enseignement et de recherche français ou étrangers, des laboratoires publics ou privés.

# Focusing Choke Ring Antenna for a Short-Range Millimeter-Wave Exposure System

A.V. Boriskin<sup>#</sup>, M. Zhadobov<sup>#</sup>, C. Person<sup>\*</sup>, and R. Sauleau<sup>#</sup>

<sup>#</sup> Institut d'Electronique et de Télécommunications de Rennes (IETR),  
UMR CNRS 6164, Université de Rennes 1, Rennes, France

<sup>\*</sup> Lab-STICC, Telecom Bretagne, Brest, France

**Abstract**— An advanced feed for a mm-wave short-range exposure system is reported. The feed configuration is optimized to provide a highly-uniform illumination of biological samples positioned close to the antenna aperture. The prototype of the antenna is fabricated in metallized foam and measured. Its near-field characteristics are studied using the infrared imaging technique. The significant advantages of the reported choke ring antenna in terms of the enhanced exposure efficiency, improved exposure uniformity, and reduced exposure distance, are demonstrated via comparison with standard open-ended waveguide and horn antennas.

**Keywords**—bioelectromagnetics, choke ring antenna, 60 GHz, dosimetry, exposure system, exposure efficiency, metallized foam

## I. INTRODUCTION

The introduction of new standards for the wireless networking in the unlicensed 60 GHz band raised certain concerns about the possible health risks associated with interactions between the millimeter waves, not present in the ambient electromagnetic background, and the human body. *In vitro* bioelectromagnetic studies is an established approach for assessing the biological impacts of electromagnetic radiations [1]. It implies a well-controlled exposure of biological samples (i.e. biological solution or cells in culture placed in a tissue plate). For this purpose, a number of exposure systems have been developed recently based on standard waveguide feeds [1-8]. The common weak points of these systems with respect to the target exposure specifications are insufficient uniformity of the power density distribution at the surface of the sample under test (SUT), and/or low exposure efficiency. Thus developing new antenna systems enabling better control over these exposure characteristics is necessary.

In this paper, we present a novel Choke Ring Antenna (CRA) designed and optimized to maximize the exposure efficiency of the exposure system, which has been developed recently at IETR, France for bioelectromagnetic studies in the 60-GHz band [5].

The advantages offered by the proposed CRA (Fig. 1), important for the target application, are the following:

- compact size, which helps minimize perturbations due to the backscattering from high-contrast biological samples,
- large opening angle, which leads to a reduced exposure distance,

This work was supported in part by ANR France under grant ANR-09-RPDOC-003-01 (project Bio-CEM), by CNRS France, and by the European Science Foundation under the RNP NEWFOCUS program.



Fig. 1. Photo of the antenna prototype attached to a standard circular-to-rectangular waveguide transition. Metallized surfaces are seen in grey color.

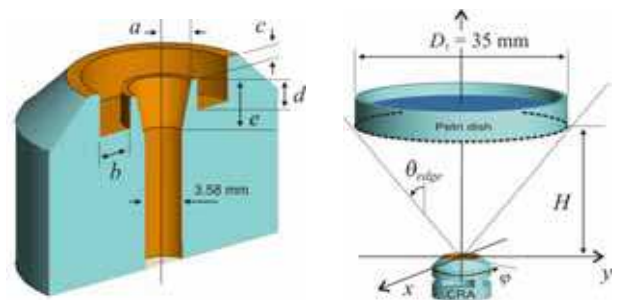


Fig. 2. Cross-sectional view of the CRA and a typical exposure scenario.

- smooth sectoral pattern, enabling the desired uniform illumination of the SUT surface,
- rotational symmetry of the radiating structure enabling both linear and circular polarization regimes,
- high radiation efficiency,
- ease of integration with a waveguide feeding system.

These advantages already made CRAs a favorable solution for various applications at lower frequencies, such as primary focus antennas for large reflectors [9,10], satellite communication [11] and GPS systems [12].

In this work, for the first time, the CRA is considered as a radiating structure for a mm-wave exposure system. The

preliminary numerical investigations into the feasibility and beam-forming capabilities of choke horn antennas assisted with rectangular gratings have been reported in [13,14]. Unlike those, the proposed circular CRA is suitable both for linear and circular polarizations. Moreover, its original design facilitated fabrication in metallized foam, which leads to a better pattern symmetry and lower side lobe level (SLL) achieved thanks to the natural suppression of the edge currents, which otherwise are induced on the metal surfaces due to the strong back-scattering from a high-contrast SUT. As to the best of our knowledge, this is one of the very first antennas in metallized foam with the operational frequency as high as 60 GHz.

## II. DESIGN PROCEDURE

The topology of the proposed CRA is presented in Fig. 2. The antenna consists of a conical horn surrounded by a choke ring whose rim is slightly extended above the horn aperture and cut under 45 degree to reinforce the structure while keeping the thickness of the metallized rim of 1 mm. The antenna is fed by a standard V-band circular waveguide with a diameter 3.58 mm and is intended to operate in the narrow band of 60 GHz  $\pm$  1%.

The antenna geometry is optimized to provide the highest possible *exposure efficiency* (i.e. the maximum ratio between the useful power incident on the SUT surface and the total radiated power). An additional restriction is applied in terms of the *exposure uniformity*: the maximum allowed variation of the incident power density at the SUT surface is limited by -0.5dB (W/m<sup>2</sup>). These specifications imply development of an antenna with high radiation efficiency, symmetrical sectoral beam, and low SLL. To meet these specifications, the following optimization procedure is followed:

- first, the CRA configuration was optimized using a cost function defined as a mismatch between the actual antenna pattern and sec<sup>2</sup> beam with a widest possible open angle (the latter requirement is imposed to minimize the exposure distance),
- second, a constant flux through the SUT surface optimization criterion is used with a target uniformity of the incident power density defined as -0.5dB (W/m<sup>2</sup>),
- finally, the exposure efficiency is calculated as a ratio of the useful power (i.e. incident on the SUT surface) to the total radiated power.

Note that the secant-square radiation pattern at far-field does not guarantee a flat symmetrical distribution at the near zone. Thus the second optimization step is essential. The analysis and optimization of the antenna configuration has been performed using a full-wave software FEKO<sup>TM</sup>.

## III. ANTENNA RADIATION CHARACTERISTICS

The optimal values of the CRA control parameters are given in Table 1, and its simulated and measured radiation patterns are shown in Fig. 3. Although the antenna is intended to operate in a narrow band, its performance is studied in a wider frequency range to compensate for the fabrication tolerances (the parametric study was reported in [15]). The CRA pattern axis ratio and half power beam width (HPBW) in both principal planes are represented in Fig. 4. The symmetry

is well preserved within the entire frequency range. At the central frequency of 60 GHz, the HPBW and beam axial ratio equal 74° and 0.98, respectively. The measured and simulated reflection coefficient is shown in Fig. 5.

TABLE I. OPTIMIZED VALUES OF THE CRA CONTROL PARAMETERS

Control parameter	<i>a</i>	<i>b</i>	<i>c</i>	<i>d</i>	<i>e</i>
Optimal value, mm	0.90	3.00	1.00	2.50	3.75

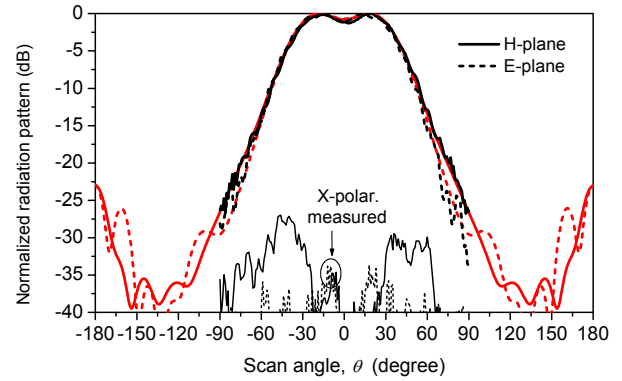


Fig. 3. Normalized radiation pattern simulated (red) and measured (black) in two principal planes at 60-GHz.

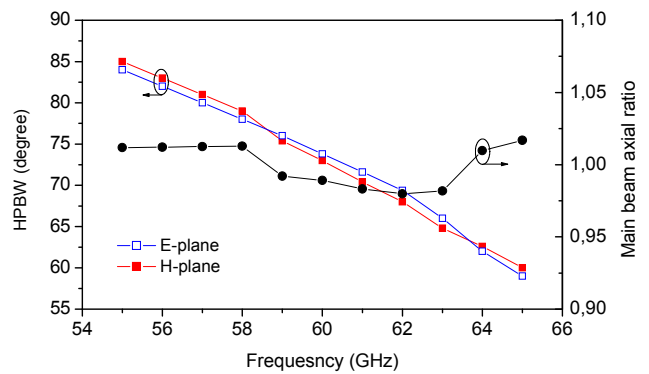


Fig. 4. Simulated HPBW and main beam axial ratio vs. frequency.

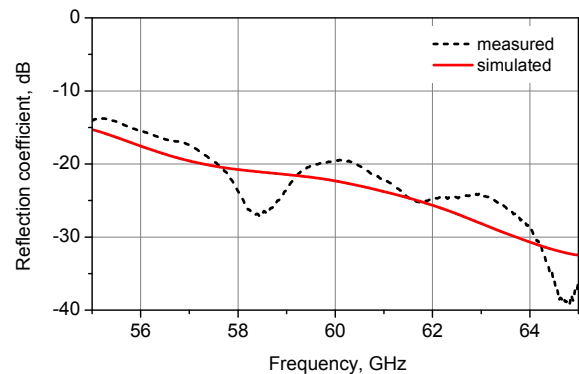


Fig. 5. CRA reflection coefficient.

The antenna prototype (Fig. 1) was fabricated in metallized foam following the procedure described in [16]. The material used for fabrication is a commercially-available dielectric foam Eccostock®LoK ( $\epsilon_r = 1.8$ ,  $\tan\delta = 0.0028$  in Ka-band). The features of the foam important for the target applications are: light weight, sufficient rigidity, and slightly rough surface, which is good for the metallization purpose. In addition, the selected foam has low water absorption, which allows one to use it inside incubators with high humidity.

The radiation efficiency of the antennas at 60 GHz is estimated as  $\sim 96\%$ . The loss budget is estimated as follows: measured reflection loss of  $\sim 1\%$  (Fig. 5) and simulated dissipation loss in the foam and silver paint of about 3%.

#### IV. ANTENNA NEAR-ZONE PERFORMANCE

The highly localized superficial absorption in water at mm-waves enables one to reconstruct the field intensity distribution on a surface of a water-based semi-solid phantom by recording the initial temperature rise rate and heating pattern on the phantom surface. In the reported study, the thermal images are recorded using a high-resolution IR camera FLIR SC5000 (FLIR Systems, Portland, OR) operating in the 2.5–5.1- $\mu\text{m}$  spectral range; its sensitivity and surface resolution are 0.025°C and 0.25 mm<sup>2</sup>, respectively. The description of the experimental set-up and methodology is presented in [17] and thus omitted here.

In the experiment, we used a semi-solid 4% -agar phantom reported in [17]. Due to the high water concentration, its permittivity is close to the permittivity of free water ( $\epsilon = 11.9 - j19.5$  at 60 GHz). The phantom was fabricated in a shape of a thin cylinder (diameter  $D_{ph} = 140$  mm, thickness  $t = 7$  mm) and illuminated from the top (Fig. 6). The thermal image was recorder by the camera, which was slightly tilted to avoid the phantom shadowing by the antenna.

A representative image of the heating pattern is shown in Fig. 7. As we can see, the dimensions and uniformity of the thermal spot are in good agreement with expectations. The slight asymmetry of the spot is due to the minor roughness of the phantom surface.

The measured temperature profile in TE plane is shown in Fig. 8 where it is superimposed with the simulated data for the field intensity distribution at the SUT surface. The excellent agreement is observed between the simulated and experimental data as well as with the target specification ( $-0.5\text{dBW/m}^2$ ) given for the edge illumination and exposure uniformity levels.

Worth mentioning that IR imaging of a Petri dish illuminated as shown in Fig. 2 is more difficult due to the high absorption of the IR spectra by the culture plate and the large dimensions of the IR camera which require development of a sophisticated experimental setup. Because of this the phantom-based imaging approach has been used.

#### V. BENCHMARKING WITH STANDARD FEEDS

Finally, the performance characteristics of the proposed CRA are compared with those of standard waveguide feeds used in earlier studies [2-8] (where appropriate, the feed dimensions are scaled to fit the 60 GHz operational frequency).

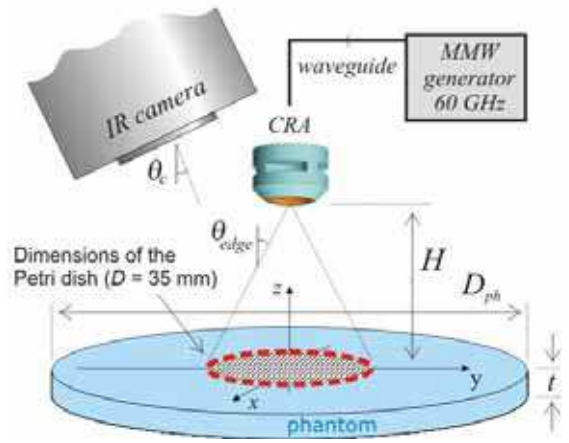


Fig. 6. Schematic drawing of the experimental set-up used for visualization of the antenna near-field pattern (not to scale).

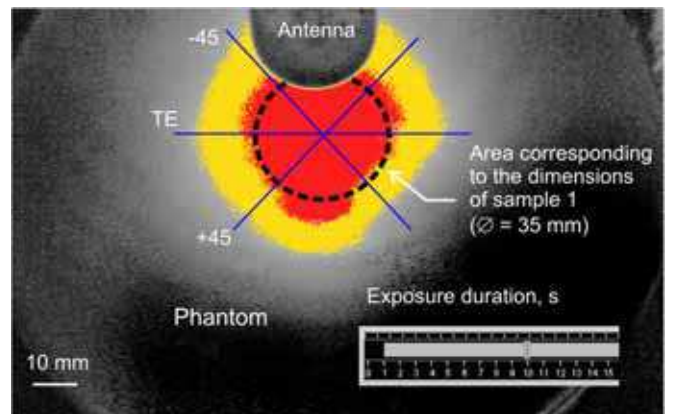


Fig. 7. Heating pattern recorder at the surface of the phantom for the CRA positioned at  $z = 48.0$  mm. The spots with -1 dB and -3 dB uniformity levels are highlighted in red and yellow colors, respectively.

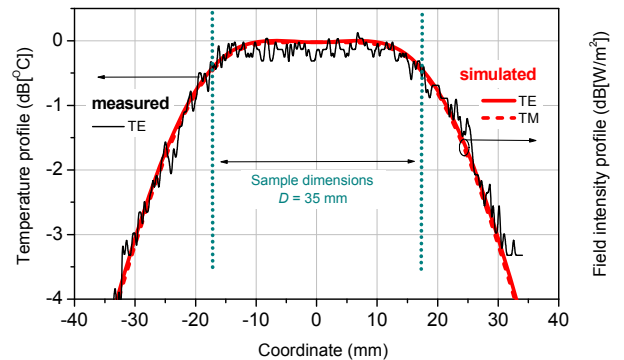


Fig. 8. Measured temperature profile (left axis) and simulated field intensity distribution (right axis). The measured curve is extracted from the heating pattern shown in Fig. 7.

The main exposure characteristics of the reference feeds and reported CRA are summarized in Table 2. As we can see, the proposed antenna significantly outperforms all the reference feeds in terms of all the exposure characteristics.

TABLE II. BENCHMARKING: PROPOSED CRA VERSUS STANDARD WAVEGUIDE FEEDS

	Rectangular waveguide WR-15	Pyramidal horn (gain 16.2 dBi)	Circular waveguide	Conical horn (gain 21.5 dBi)	Proposed CRA
-0.5 dB(W/m <sup>2</sup> ) exposure uniformity					
- exposure distance, mm	95	270	95	380	46
- main beam axial ratio, a.u.	0.85	0.29	0.98	1.16	0.98
- max exposure level *, V/m	394	170	227	226	480
- exposure efficiency, %	27.8	27.6	30.0	37.4	55.8
-1.0 dB(W/m <sup>2</sup> ) exposure uniformity					
- exposure distance, mm	68	210	66	265	40
- main beam axial ratio, a.u.	0.83	0.37	0.98	1.16	0.98
- max exposure level *, V/m	550	211	330	320	550
- exposure efficiency, %	36.8	34.5	40.3	48.5	63.0

\* - Total input power is 1W .

### CONCLUSIONS

An advanced focusing CRA with enhanced exposure efficiency has been designed and prototyped in metallized foam. A very good agreement between the simulated and measured characteristics has been obtained confirming the credibility of the selected design and fabrication methodologies.

Compared to the standard waveguide feeds, a two-fold advantage in terms of exposure efficiency has been achieved thanks to the improved beam symmetry and exposure uniformity. Advanced exposure characteristics together with the reduced exposure distance make proposed CRA an excellent candidate for BEM experiments in the 60-GHz band.

Additional information about the antenna optimization procedure and its performance characteristics is presented in the recent paper [18].

### REFERENCES

[1] M. Zhadobov, N. Chahat, R. Sauleau, C. Le Quément, and Y. Le Dréan, "Millimeter-wave interactions with the human body: state of knowledge and recent advances," *Int. J. Microwave Wireless Technol.*, vol. 3, pp. 237–247, 2011.

[2] J.X. Zhao, "Numerical dosimetry for cells under millimetre-wave irradiation using Petri dish exposure set-ups," *Phys. Med. Biol.*, vol. 50 pp. 3405–3421, 2005.

[3] J. Zhao and Z. Wei, "Numerical modeling and dosimetry of the 35 mm Petri dish under 46 GHz millimeter wave exposure," *Bioelectromagnetics*, vol. 26, no. 6, pp. 481–488, 2005.

[4] M. Zhadobov, R. Sauleau, V. Vié, M. Himdi, L. Le Coq, D. Thouroude, "Interactions between 60-GHz millimeter waves and artificial biological membranes: dependence on radiation parameters," *IEEE Trans. Microwave Theory Tech.*, vol. 54, no. 6, pp. 2534–2542, Jun. 2006.

[5] M. Zhadobov, Ch. Nicolas Nicolaz, R. Sauleau, F. Desmots, D. Thouroude, D. Michel, and Y. Le Dréan, "Evaluation of the potential biological effects of millimeter waves at 60.42 GHz upon human cells," *IEEE Trans. Antennas Propag.*, vol. 57, no. 10, pp. 2949–2956, 2009.

[6] S. Kurogi, H. Saito, T. Taguchi, Y. Suzuki, and M. Taki, "Development and dosimetry of a free-space type in vitro exposure apparatus for millimeter-waves," in *Proc. Int. Symp. Electromagnetic Compatibility (EMC)*, Kyoto, Japan, 2009, 22S1-2.

[7] P. Siegel and V. Píkov, "Impact of low intensity millimeter waves on cell functions," *Electron Lett.*, vol. 46, no. 26, pp. 70–72, 2010.

[8] M. Zhadobov, R. Sauleau, R. Augustine, C. Le Quément, Y. Le Dréan, and D. Thouroude, "Near-field dosimetry for in-vitro exposure of human cells at 60 GHz," *Bioelectromagnetics*, vol. 33, no. 1, pp. 55–64, 2012.

[9] R. Wohlleben, H. Mattes, and O. Lochner, "Simple small primary feed for large opening angles and high aperture efficiency," *Electronics Lett.*, vol. 8, no. 19, pp. 474–476, 1972.

[10] L. Shafai and A.A. Kishk, "Prime focus waveguide feeds," in *Microwave Horns and Feeds*, A.D. Olver (ed.), IEEE Press, 1994.

[11] J. Galvan and D. Colantonio, "Low back radiation compact antenna for data downlink in LEO satellites," in *Proc. Int. Microwave Optoelectronics Conf. (IMOC)*, 2009, Belem, Brazil, pp. 816–820.

[12] F. Sciré-Scappuzzo and S.N. Makarov, "A low-multipath wideband GPS antenna with cutoff or non-cutoff corrugated ground plane," *IEEE Trans. Antennas Propag.*, vol. 57, no. 1, pp. 33–46, Jan. 2009.

[13] S. Steshenko, A.A. Kirilenko, A.V. Boriskin, M. Zhadobov, and R. Sauleau, "Advanced modeling of choke ring antennas for mm-wave applications," in *Proc. Eur. Conf. Antennas Propag. (EuCAP)*, Prague, *Czech Republic*, 2012, pp. 650–654.

[14] S. Steshenko, A.A. Kirilenko, A.V. Boriskin, M. Zhadobov, and R. Sauleau, "H-plane radiation patterns of rectangular waveguide aperture with a corrugated flange," in *Proc. Int. Conf. Math. Methods in Electromagnetic Theory (MMET)*, Kharkov, 2012, pp. 476–479.

[15] A.V. Boriskin, M. Zhadobov, R. Sauleau, and Y. Le Drean, "Choke ring antenna for bioelectromagnetic experiments at 60 GHz," in *Proc. 7th European Conf. Antennas Propag. (EuCAP-13)*, Goteborg (Sweden), 2013, pp. 2566–2568.

[16] A. Rolland, A.V. Boriskin, C. Person, L. Le Coq, and R. Sauleau, "Lens-corrected axis-symmetrical shaped horn antenna in metallized foam with improved bandwidth," *IEEE Antennas Wireless Propag. Lett.*, vol. 11, no. 1, pp. 57–60, 2012.

[17] N. Chahat, M. Zhadobov, R. Sauleau, and S.I. Alekseev, "New method for determining dielectric properties of skin and phantoms at millimeter waves based on heating kinetics," *IEEE Trans. Microwave Theory Tech.*, vol. 60, no. 3, pp. 827–832, Mar. 2012.

[18] A.V. Boriskin, M. Zhadobov, S. Steshenko, Y. Le Drean, C. Pearson, and R. Sauleau, "Enhancing exposure efficiency and uniformity using a choke ring antenna: application to bioelectromagnetic studies at 60 GHz," *IEEE Trans. Microwave Theory Tech.*, vol. 61, no. 5, pp. 2005–2014, May 2013.